Fracture characteristics of bulk metallic glass under high speed impact*

Sun Bao-Ru(孙宝茹), Zhan Zai-Ji(战再吉)†, Liang Bo(梁 波), Zhang Rui-Jun(张瑞军), and Wang Wen-Kui(王文魁)

State Key Laboratory of Metastable Materials Science and Technology, Yanshan University, Qinhuangdao 066004, *China*

(Received 31 May 2011; revised manuscript received 1 November 2011)

High speed impact experiments of rectangular plate-shaped $Zr_{41}Ti_{14}Cu_{12.5}Ni_{10}Be_{22.5}$ bulk metallic glass (BMG) were performed using a two-stage light gas gun. Under spherical shock waves with impact velocities ranging from 0.503 km/s to 4.917 km/s, obvious traces of laminated spallation at the back (free) surface and melting (liquid droplets) at the impact point were observed. The angles about 0°, 17°, 36°, and 90° to the shocking direction were shown in the internal samples because of the interaction between the compressive shock waves and the rarefaction waves. The compressive normal stress was found to induce the consequent temperature rise in the core of the shear band.

Keywords: bulk metallic glass, shock wave, shear cracks/bands

PACS: 61.43.Dq, 62.20.M–, 62.50.–p **DOI:** 10.1088/1674-1056/21/5/056101

1. Introduction

The multicomponent $Zr_{41}Ti_{14}Cu_{12.5}Ni_{10}Be_{22.5}$ bulk metallic glass (BMG) has recently gained considerable attention due to its extremely high glass forming ability and high fracture toughness.[1−3] Commercial applications in making golf clubs, kinetic energy penetrators, and bearings for a space environment[4] have been reported. The dynamic response of the BMG is of considerable interest for gaining insight into the high strain-rate response of this type of materials and for potential applications. The dynamic compression of various BMGs has been investigated in several studies.[5−13] For a Zr-based BMG, i.e., $Zr_{41.25}Ti_{13.75}Ni_{10}Cu_{12.5}Be_{22.5}$, Lu reported that the strengths under dynamic and quasi-static loading conditions were quite similar, and the failure was characterized by a predominantly inhomogeneous inelastic flow.[13] The strain-rate softening behavior has been reported in both $Zr_{57}Ti_5Cu_{20}Ni_8Al_{10}$ and $Zr_{41.25}Ti_{13.75}Ni_{10}Cu_{12.5}Be_{22.5}$ BMGs.[14] Such a behavior was also investigated when the zirconium was replaced by hafnium.[4] Even though the deformation and the damage mechanisms of the BMGs under moderate dynamic loading conditions have received extensive investigation, only a few studies addressed the shock response of the BMG. Bach *et al.* studied the shock wave consolidation of metallic glass powder, they investigated the effects of the shock wave energy and the shock wave duration.[15] Conner *et al.* investigated the high strain rate behavior of fiber-reinforced $Zr_{41.2}Ti_{13.8}Cu_{12.5}Ni_{10}Be_{22.5}$ composites, and demonstrated their potential application as armor penetrators.[16] Yang *et al.* employed a two-stage light gas gun to study the effects of planar shock compression on the void formation and the cracking in a Zr-based BMG ($Zr_{41}Ti_{14}Cu_{12.5}Ni_{10}Be_{22.5}$) under hypervelocity impact conditions.[8] Yang *et al.* used a two-stage light gas gun to further investigate the damage features of $Zr_{41}Ti_{14}Cu_{12.5}Ni_{10}Be_{22.5}$ subjected to the hypervelocity impact. The results from scanning electron microscopy showed that both radial and symmetric cracks were formed on the shocked surface of the target plate when impacted by an aluminum flyer with an impact velocity of 2.7 km/s. Shear bands/cracks parallel to each other on the cross section close to the shocked surface of the target were also observed.[9]

To date, the physical mechanism of the dynamic failure in the BMG remains unclear. However, the characterization of the dynamic failure behavior of this material is very important for its potential engineering applications. The current research mainly deals with the dynamic behavior of the rod-shaped BMG at the low or medium strain rate response regime. A further investigation of the dynamic be-

*Project supported by the National Basic Research Program of China (Grant No. 2010CB731600).

†Corresponding author. E-mail: zjzhan@ysu.edu.cn

© 2012 Chinese Physical Society and IOP Publishing Ltd

havior is undoubtedly necessary. So in this paper, we focus on the fracture characteristics of rectangular plate-shaped $Zr_{41}Ti_{14}Cu_{12.5}Ni_{10}Be_{22.5}$ BMG under a high speed impact.

2. Experiments

Ingots of the alloy with a nominal composition of $Zr_{41}Ti_{14}Cu_{12.5}Ni_{10}Be_{22.5}$ were prepared by mixing pure elements in an arc-melting furnace under Ti-gettered argon atmosphere. The purities of Zr, Ti, Cu, Ni, and Be were 99.9%, 99.9%, 99.5%, 99%, and 99.5%, respectively. Properties of the BMG employed in the experiments are shown in Table 1. The ingots were then cast into BMG plates with dimensions of 50 mm (length) ×30 mm (width) ×5 mm (thickness). The plates were used as targets for high speed impact experiments. Structures of the samples before and after the high speed impact experiments were analyzed by using the X-ray diffraction (XRD). Spherical aluminum projectiles (3.1 mm in diameter) were fired at the speeds of 0.503 km/s, 0.708 km/s, 1.085 km/s, 1.507 km/s, 2.081 km/s, 3.076 km/s, 4.083 km/s, and 4.917 km/s respectively by using a two-stage light gas gun. The pressure difference between the launch tube and the target compartment was 2 kPa. The sizes of the projectiles were much smaller than that of the BMG target (medium thickness target) used in this study. The speeds were measured by a laser speed system. Figure 1 shows the schematic diagram of the experimental device.

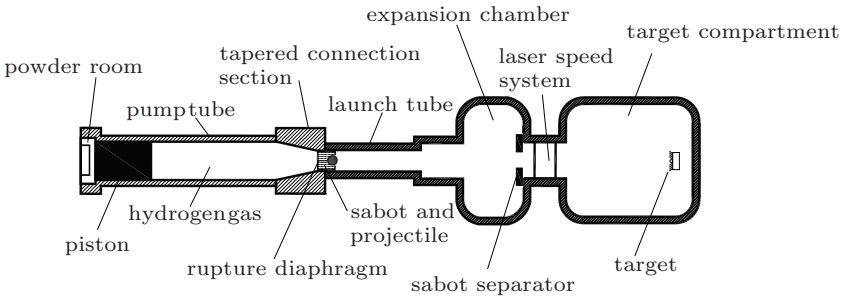


Fig. 1. Schematic diagram of two-stage light gas gun.

Table 1. Properties of the BMG employed in experiments.

Thermal conductivity /W·m^{-1}·K^{-1}	Heat capacity, /J(g· K)$^{-1}$	Density /g.cm^{-3}	Young's modulus/GPa	Shear modulus/GPa
3.5[17]	23[13]	6.128[18]	96[13]	37.17[18]
Bulk modulus/GPa	Elasticstrain	Tensile strength/GPa	Vickers hardness /kg·mm^{-2}	Viscosity coefficient /Pa·s
105.4[18]	∼2.0%[13]	1.9[13]	534[13]	4.0×10^{-5}[18]

3. Results and discussion

The impacted specimens were cut out from the plates using an electric spark-cutting machine, then grounded and polished mechanically. The morphologies of the impacted craters and the fracture characteristics of the surfaces and the cross sections of the recovered targets were observed by using a KYKY-2800 scanning electron microscopy (SEM).

Structures of the samples before and after the high speed impact experiments are shown in Fig. 2. The broad diffraction maxima in the XRD curves show the characteristics of an amorphous structure. No evidence of phase separation is found in these samples.

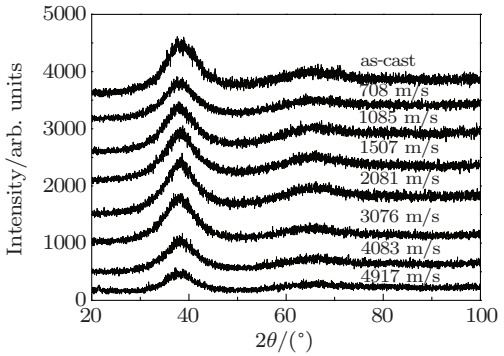


Fig. 2. XRD patterns of samples before and after the high speed impact experiments.

The impact pressure and the velocity are shown in Fig. 3. Photographs of the typical specimens re-

covered after the impact are shown in Fig. 4. As shown in Fig. 4(a), microcracks can be found in the recovered specimens impacted at the lower velocities of 0.503 km/s and 0.708 km/s, and the targets do not fail in these cases. The specimens are fractured and fail gradually at the velocities of 1.085–3.076 km/s (Figs. 4(b) and 4(c)). When the velocity reaches 4.083 km/s (Fig. 4(d)), the specimens are fractured into many pieces and fail completely. At 4.083 km/s, the impact end is completely fractured into many pieces, and a fragment is fractured off in a cone shape; this was also observed by Morgana in rod samples at high strain rate.[12] Most probably it is the result of the interaction between the compressive shock waves and the rarefaction waves reflected from the back and the lateral surfaces. The samples impacted at the velocities of 1.085 km/s and 3.076 km/s show annular cracks and densely distributed radial cracking initiating from the impact point of the impact face; such a behavior was also observed by Yang *et al.*[9] Because the targets are of the medium thick type and the projectiles are spherical, a compressive shock wave acts initially on the impact point of the BMG target and induces the high strain, which leads to the radial cracking and the annular cracks.

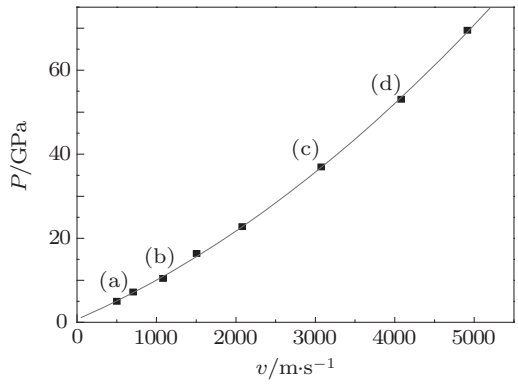


Fig. 3. The polynomial fit curve of the impact pressure versus velocity, the points labelled corresponding to the photographs shown in Fig. 4.

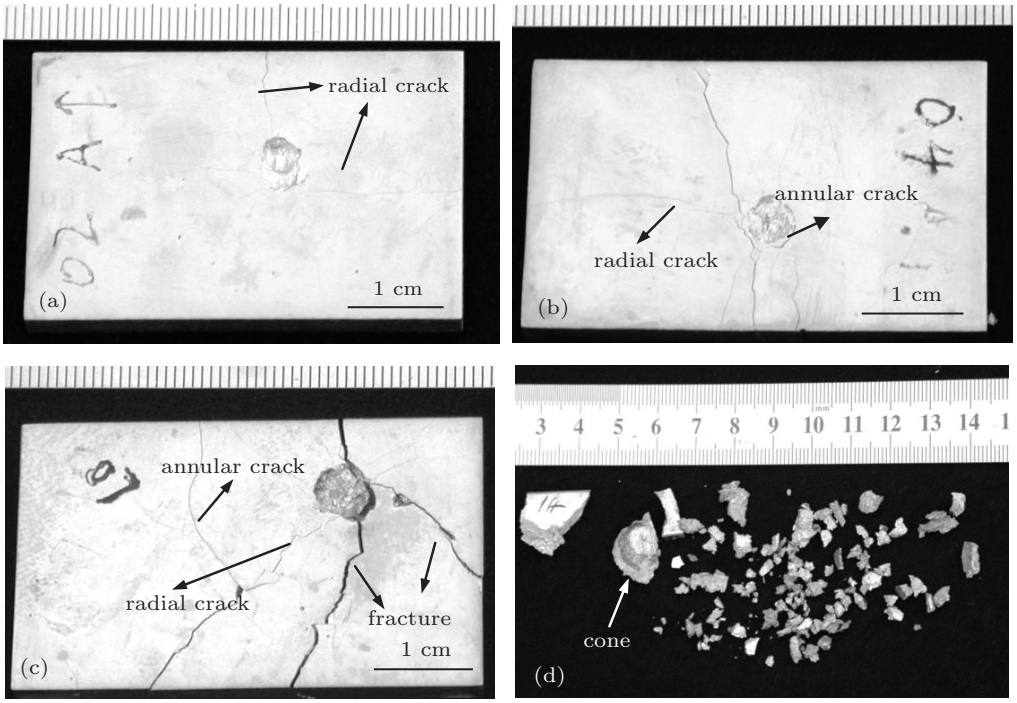


Fig. 4. Photographs of typical specimens impacted at the velocities of (a) 0.708 km/s, (b) 1.085 km/s, (c) 3.076 km/s, and (d) 4.083 km/s.

Figure 5 shows the craters, the cracks, and the fracture surface, which are formed on the top, the back, and the lateral surfaces of the BMG impacted by spherical aluminum projectiles at the velocity of 0.708 km/s. The craters are formed on the top surface of the BMG (Fig. 5(a)). The shape of the crater is almost spherical without any obvious outer projecting fringe at the mouth of the crater. This is related to the high strength and low ductility of the BMG material. The crater becomes more spherical with the increase of the projectile velocity; such a behavior was also observed by Yang *et al.*[9] The sample back (free) surface presents the phenomenon of lamination spallation (Fig. 5(b)). Figure 5(c) indicates the cracks on the sample lateral surface caused by the impact. It can be seen that several fracture planes (shear cracks/bands)

appear on the lateral surface, and the dominating angles to the shock direction are approximately 0°, 17°, 36°, and 90° (Fig. 5(c)). The main observations took place under compressive loading with the formation of shear bands in bulk amorphous alloys in the range of 45° to 55° to the loading direction. Figure 5(d) shows the enlarged A region in Fig. 5(b), a few vein patterns are observed, and the fracture surface presents the brittle fracture, which indicates that the temperature is low at the moment of fracture.

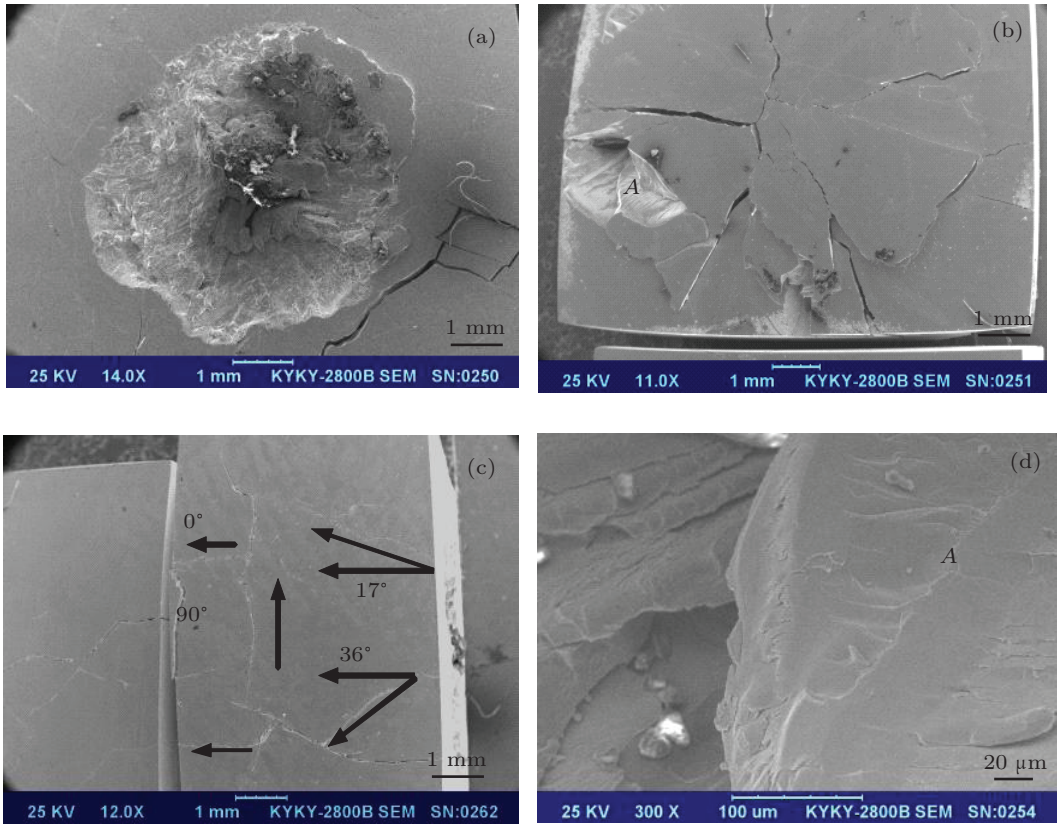


Fig. 5. Micrographs of (a) crater, ((b), (c)) cracks, and (d) fracture surface. The BMG is impacted by spherical aluminum projectiles at the velocity of 0.708 km/s. Panel (d) shows the enlarged A region in panel (b).

The micrographs of the crater bottoms on the surfaces of the recovered specimens are shown in Fig. 6 to investigate the damage induced by high speed impacts. At relatively low impact velocities (Figs. 6(a) and 6(b)), liquid droplets and disorganized dimple patterns typical appeared at the dynamically fractured surfaces in BMGs can be found. However, when the impact velocity is increased to 4.083 km/s, the dimple patterns vanish (Fig. 6(c)).

The average strain rate during the dynamic compression can be estimated from the ratio between the impact velocity and the diagonal size of the indentation.[19] In the current study, the average strain rates are varied from 1.4×10^5 s^{-1} to 9.8×10^5 s^{-1}. The indentation loads are in the range of 7.18 GPa to 69.45 GPa. Employing the analytical method of Zhang *et al.*[20], we find the temperature to be about 5.0×10^2 K when the impact velocity and the pressure are 0.708 km/s and 7.18 GPa, respectively. The temperature is about 1.0×10^3 K when the velocity and the pressure reach 1.085 km/s and 11.40 GPa, respectively. When the impact velocity and the pressure are as high as 4.083 km/s and 69.45 GPa, respectively, the temperature is far greater than 1.0×10^3 K, i.e., much higher than the melting point of the target, so the impact point shows the remelting phenomenon. As shown in Fig. 1, the remelting point is amorphous. This might be interpreted by the fact that with the velocity increasing, severe melting occurs, and the impact point may even be completely melted. At the same time, some holes with sizes of several hundred micrometers are also generated because of the rapid solidification (Fig. 6(c)).

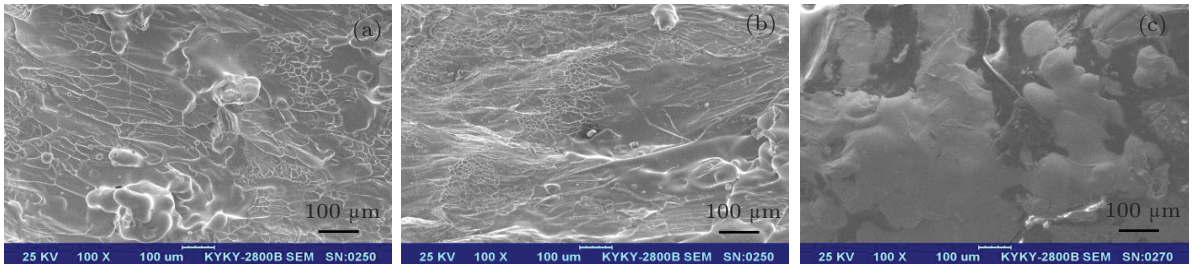


Fig. 6. SEM micrographs of the crater bottoms impacted by spherical projectiles at the velocities of (a) 0.708 km/s, (b) 1.085 km/s, and (c) 4.083 km/s.

Figure 7 shows the SEM micrographs of the fragment impacted by spherical projectiles at the velocity of 1.085 km/s. Region I is near the beneath impact point, Region III is far away from the beneath impact point (Fig. 7(a)). Clearly softened failure surfaces can be seen in regions I and II (Figs. 7(b) and 7(c)), while no obviously softened phenomenon can be observed in region III (Fig. 7(d)). These results clearly indicate the dominant effect of the compressive normal stress on the consequent temperature rise in the core of the shear band. Because of the poor heat conductivity of the BMG, the temperatures in the areas away from the impact point are low, so the morphologies of the fracture surfaces are different. We can infer that the softening degree of the fracture surface is an important factor for the morphology, i.e., it is easy to form veinal patterns at low softening degrees, contrary to that, it is easy to form dimple patterns.

The tensile behavior is shown in Fig. 7(b). It is related to the tensile action between the compressive shock wave and the rarefaction wave from the back surface. The enlarged crack tip (region D in Fig. 7(e)) indicates that the incorporation of holes induces the extending of the cracks.

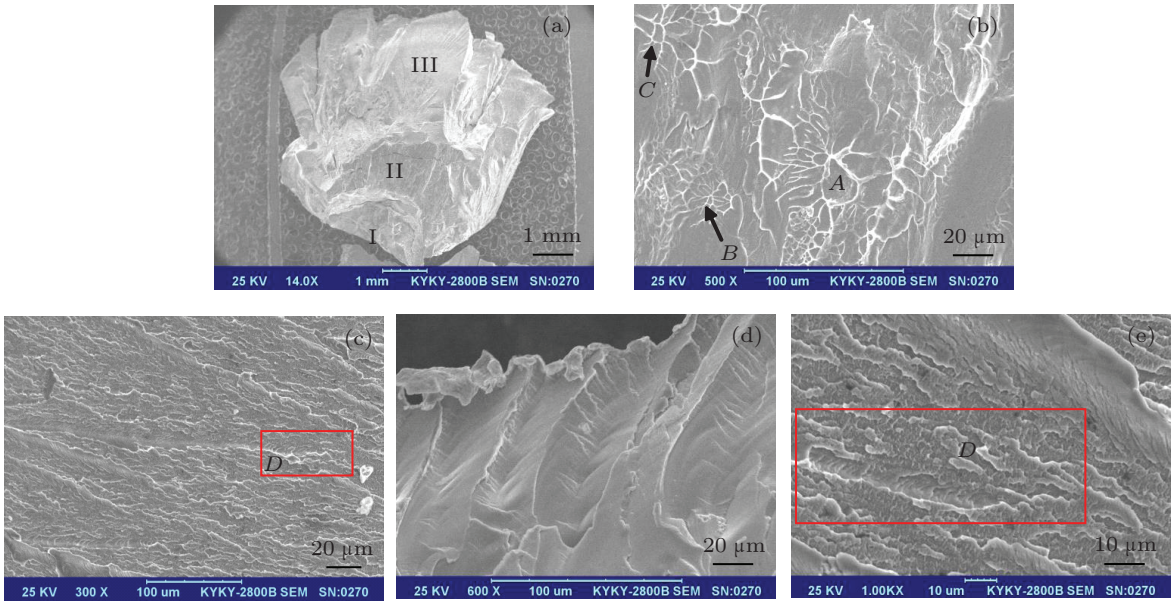


Fig. 7. (colour online) SEM micrographs of the fragment impacted by spherical projectiles at the velocity of 1.085 km/s. The fragment in panel (a) is divided into three regions (I, II, III), panels (b), (c), and (d) show the enlarged three regions, respectively, and panel (e) is the enlarged region D in panel (c).

From the above experimental observation, it can be summarized that the fracture model of the BMG under high speed impact is the result of complex stresses, which are formed by the interaction between the compressive shock waves and the rarefaction waves reflected from the back and the lateral surfaces. For crystal metals, microvoids firstly start nucleating in the material weaknesses (grain boundary, interfaces of two phase particle, etc.) under the dynamic loading, and then those voids start to grow un-

der the tensile stress. When the voids grow to a certain extent, they start through and result in the formation of macroscopic fracture surface inside the material.[21−23] The BMG is totally different from the crystal metal in the array of atoms. It has no grain or boundary. It is uniphase and has an amorphous structure. The regime of stress concentration within the specimen causes the inhomogeneous deformation. According to Speapen's free volume based model, the deformation is usually accompanied by changes in the number of free volumes. At room temperature, a large number of free volumes result to meet the need for deformation with the increasing of the loading stress. Due to the short loading time and the weak relaxation effect, the free volumes increase to a certain degree of aggregation, and then the microvoids are formed inside the BMG specimens. The formation of shear cracks/bands is most likely related to the nucleation, growth, and coalescence of the microvoids during the compression or tension. The size and the number of the shear cracks/bands increases slightly with the increase of the loading stress. At the same time, the accumulation of the free volumes in the shear zone reduces the viscosity of the amorphous phase and the yield strength. Under the external force, the fracture zone occurs along the shear cracks/bands of lower viscosity. Figure 8 indicates the formation process of cracks in the BMG target under shock loading induced by the impact of a high speed projectile.

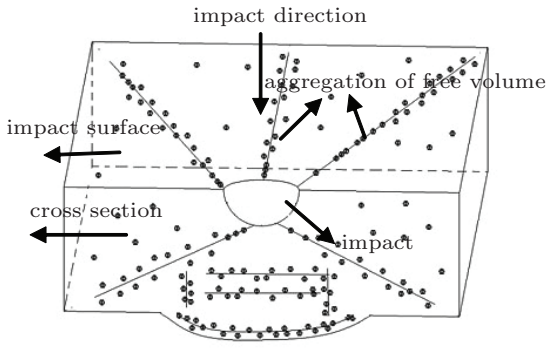


Fig. 8. Formation mechanism of shear bands/cracks in BMG under shock loading.

4. Conclusion

In this paper, the effect of the impact velocity on the fracture characteristics of the $Zr_{41}Ti_{14}Cu_{12.5}Ni_{10}Be_{22.5}$ BMG is investigated by using a two-stage light gas gun. The results demonstrate that the lamination spallation appears because of the interaction between the compressive shock waves and the rarefaction waves reflected from the back and the lateral surfaces. The samples fail at different angles between the shocking directions, which is different from that in the quasi-static uniaxial compressive or tensile tests. Evidence of melting (liquid droplets) due to the high strain rate deformation is also observed at the impact point. A coupling effect of thermal and mechanics is present during the dynamic damage. The dominant effect of the compressive normal stress on the consequent temperature rise in the core of the shear band is observed. The dimple and the veinal patterns observed at different locations are believed to be affected by the softening degree and the temperature. The accumulation of the free volumes in the shear zone reduces the viscosity of the amorphous phase and the yield strength. Under the external force, the fracture zone occurs along the shear cracks/bands of low viscosity.

Acknowledgements

The authors gratefully acknowledge the China Aerodynamics Research and Development Center for providing the two-stage light gas gun. We also thank Dr. Zhang Bao-Qing and Dr. Shi An-Hua for the assistance in the sample preparation.

References

[1] Tang X P, Geyer U, Busch R, Johnson W L and Wu Y 1999 *Nature* **402** 160

[2] Wei H Q, Long Z L and Zhang Z C 2009 *Acta Phys. Sin.* **58** 2556 (in Chinese)

[3] Dai L H, Liu L F, Yan M and Wei B C 2004 *Chin. Phys. Lett.* **21** 1593

[4] Subhash G, Dowding R and Kecskes L 2002 *Mater. Sci. Eng.* A **334** 33

[5] Liu L F, Dai L H and Bai Y L 2008 *Chin. Phys. Lett.* **25** 1052

[6] Conner R, Choi-Yim H and Johnson W 1999 *J. Mater. Res.* **14** 3292

[7] Nathenson D 2006 *Experimental Investigation of High Velocity Impacts on Brittle Materials* (Ph. D. dissertation) (Cleveland: Case Western Reserve University) p. 78

[8] Yang C, Liu R P, Zhang B Q, Wang Q, Zhan Z J, Sun L L, Zhang J and Gong Z Z 2005 *J. Mater. Sci.* **40** 3917

[9] Yang C, Wang W K, Liu R P, Zhang X Y and Li X 2006 *Journal of Spacecraft and Rockets* **43** 565

[10] Zhuang S M, Lu J and Ravichandran G 2002 *Appl. Phys. Lett.* **80** 4522

[11] Mukai T, Nieh T, Kawamura Y, Inoue A and Higashi K 2002 *Intermetallics* **10** 1071

[12] Morgana M 2008 *Quasar Structure from Microlensing in Gravitationally Lensed Quasars* (Ph. D. dissertation) (Atlanta: Georgia Institute of Technology) pp. 14–28

[13] Lu J 2002 *Mechanical Behavior of a Bulk Metallic Glass and its Composite over a Wide Range of Strain Rates and Temperatures* (Ph. D. Dissertation) (Pasadena: California Institute of Technology) pp. 172–177, p. 54

[14] Hufnagel T C, Jiao T, Li Y, Xing L Q and Ramesh K T 2002 *J. Mater. Res.* **17** 1441

[15] Bach J, Krueger B and Fultz B 1991 *Mater. Lett.* **11** 383

[16] Conner R D, Dandliker R B, Scruggs V and Johnson W L 2000 *International Journal of Impact Engineering* **24** 435

[17] Bruck H A, Rosakis A J and Johnson W L 1996 *J. Mater. Res.* **11** 503

[18] Yang C 2005 *The Shock Wave Effect of ZrTiCuNiBe Bulk Metallic Glass* (Ph. D. Dissertation) (Qinhuangdao: Yanshan University) pp. 24–33

[19] Subhash G 2000 *ASM Handbook, Mechanical Testing and Evaluation, ASM International* **8** 519

[20] Zhang H W, Spandan M and Subhash G 2008 *J. Mech. Phys. Solids* **56** 2171

[21] Seaman L, Curran D R and Shockey D A 1976 *J. Appl. Phys.* **47** 4814

[22] Deng X L, Zhu W J, Song Z F, He H L and Jing F Q 2009 *Acta Phys. Sin.* **58** 4772 (in Chinese)

[23] Wang F, Peng X S, Liu S Y, Li Y S, Jiang X H and Ding Y K 2011 *Chin. Phys.* B **20** 065202